VICTORIA UNIVERSITY OF WELLINGTON TE HERENGA WAKA NEW ZEALAND
Archives of Sustainable Energy Systems
https://www.wgtn.ac.nz/sustainable-energy-systems

Assessing the impact of solar PV on vegetation growth through ground sunlight distribution at a solar farm in Aotearoa New Zealand

Matlotlo Magasa Dhlamini, Alan Colin Brent

Abstract

The global shift toward renewable energy has positioned solar photovoltaics (PV) as central to sustainable development. However, the land demands of ground-mounted PV systems raise concerns about competition with agriculture, particularly in regions with limited or productive farmland. Agrivoltaics, which integrates solar energy generation with agricultural use, offers a potential solution. While agrivoltaics has been extensively studied in arid and semi-arid climates, little is known about its feasibility and impacts in temperate maritime climates such as Aotearoa New Zealand, particularly the effects of PV-induced shading on ground-level light availability and vegetation. This study modelled the spatial and seasonal distribution of ground-level irradiation and Photosynthetic Photon Flux Density (PPFD) beneath fixed-tilt PV arrays at Tauhei Solar Farm in the Waikato region. Using 2018 hourly SolarGIS data and a Python-based simulation, the research accounts for solar geometry, panel shading, and irradiance decomposition. It quantifies and maps PPFD to evaluate light conditions and its implications for vegetation growth. Results reveal significant spatial and temporal variation in PPFD. In summer, midday inter-row areas exceeded 450 μmol/m^2/s, while winter under-panel zones often fell below 100 μmol/m^2/s—near the light compensation point for many shade-sensitive plants. This variation supports a precision agrivoltaic strategy that zones land based on irradiance levels. By aligning crop types and planting schedules with seasonal light profiles, land productivity and ecological value can be improved. Spring and summer favour high-light crops, while winter is more suitable for shade-tolerant species or grazing. These findings are highly applicable in Aotearoa New Zealand's pasture-based systems and show that effective light management is critical for agrivoltaic success in temperate climates.

Keywords: Agrivoltaics, Irradiance modelling, Photosynthetic Photon Flux Density.

1. Introduction

Aotearoa New Zealand is steadily working towards decarbonising industries and is committed to achieving net-zero greenhouse gas (GHG) emissions by 2050 (MfE, 2024). Part of this plan includes a focus on expanding renewable energy systems. There is a relatively high projected growth of utility-scale in the coming years (Concept Consulting, 2023), which will increase the demand on productive land (Brent and Iorns, 2024).

Agrivoltaics has emerged as a promising response to this concern (Brent, 2024). It refers to the integration of solar energy production with agricultural activity, where crops or pasture can coexist with solar arrays. By integrating solar arrays with crop cultivation or livestock grazing, agrivoltaic systems aim to optimise dual land use and improve overall land-use efficiency. The integration of solar PV farms into Aotearoa New Zealand's renewable energy landscape plays a significant role in achieving the country's net-zero carbon goals. However, while solar power is growing, it remains a relatively new industry, and the study of its ecological effects, particularly on vegetation is limited. This research investigates how solar PV affects local vegetation growth through a spatial-temporal study of solar irradiation distribution, thereby contributing to a broader understanding of agrivoltaic systems and which vegetation types can thrive under them.

Aotearoa New Zealand's Ministry for the Environment (MfE, 2024) and the Government's Energy Strategy (MBIE, 2023) both emphasise the need to minimise environmental impacts while expanding renewable energy. These frameworks target 100% renewable electricity by 2030 and underscore the value of sustainable energy-land integration. The shift to 100% renewable energy raises the challenge of land competition. Solar installations may occupy 0.5% to 5% of total land according to van de Ven et al. (2021). For a geographically small country like Aotearoa New Zealand with significant protected areas, this creates challenges that agrivoltaics may help resolve. Agrivoltaic systems must ensure that agricultural and indigenous vegetation are not negatively affected, and this research contributes to that goal by providing evidence-based insights on light availability and plant suitability.

While agrivoltaics is gaining traction globally, its effectiveness in temperate maritime climates like Aotearoa New Zealand remains underexplored. This gap makes it difficult for stakeholders here to make informed decisions on co-locating solar farms with agriculture. Fixed-tilt PV utility-scale solar farms are prominent in Aotearoa New Zealand, yet little is known about how these structures influence ground-level light conditions and, by extension, the types of vegetation that can thrive beneath them. Without this knowledge, land-use decisions, vegetation planning, and policy development remain challenging.

1.1. Objective of the paper

The objective of this paper is to simulate the spatial and seasonal distribution of ground-level Photosynthetic Photon Flux Density (PPFD) beneath fixed-tilt photovoltaic (PV) arrays at Tauhei solar farm in Aotearoa New Zealand's Waikato region. By applying real irradiance data and a custom Python-based model, the study quantifies how sunlight varies throughout the year and evaluates its impact on vegetation suitability under solar infrastructure.

This paper addresses a regional research gap by offering data-driven insights on agrivoltaics in a temperate climate. It aims to inform land-use planning, crop selection, and system design by answering the following:

- How does the fixed-tilt PV array influence the spatial and seasonal distribution of PPFD?
- What proportion of land receives high, moderate, or low irradiance?
- Which vegetation types are best suited to each irradiance zone?
- What are the implications for agrivoltaic design and land-use policy in the Aotearoa New Zealand context?

The study assumes that environmental conditions at the Tauhei solar farm are representative of similar areas across the country. A flexible, exploratory approach was adopted to reflect the novel and site-specific nature of the research, allowing the methodology to evolve in response to patterns and knowledge gaps identified in the literature.

2. Literature review

This section explores the interaction between solar photovoltaic (PV) systems and vegetation, with a focus on how PV-induced shading affects ground-level light distribution and plant growth. The review adopts a scoping approach to synthesise emerging knowledge across disciplines and to identify relevant modelling techniques and

knowledge gaps, especially concerning fixed-tilt PV systems in temperate climates such as Aotearoa New Zealand.

While numerous models such as the Solar and Longwave Radiation Model (SLRM) and the GECROS crop model have successfully simulated PV impacts on crops, research tailored to temperate maritime climates remains limited, highlighting a need for regionalised agrivoltaic studies.

2.1. Review methodology

A scoping review methodology was applied based on Arksey and O'Malley (2005), complemented by Levac et al. (2010) for enhanced analytical depth. The central research question was: What is known about the impacts of solar PV installations on vegetation growth, light distribution, and microclimatic modification?

Sub-questions focused on vegetation types, modelling techniques, and regional gaps. A pragmatic and inductive approach guided the process, allowing flexible integration of literature insights into modelling design. Rather than statistical meta-analysis, a narrative synthesis was used to explore how PV systems influence ecological conditions and to inform vegetation suitability under PV structures.

The search included academic and grey literature across databases such as Scopus, ScienceDirect, Google Scholar, and Te Waharoa (Victoria University of Wellington Library). Search terms included combinations of "agrivoltaics", "solar PV and vegetation", "light distribution under solar panels", and "microclimate under PV arrays". Boolean operators (e.g., "AND", "OR") refined the queries.

Of the 1,300 initial documents identified, 41 were shortlisted after screening, and 36 met the final inclusion criteria. These were selected based on their relevance to themes such as shading, microclimate effects, light distribution, and in relation to agrivoltaics in general.

The reviewed studies were published from 2021 to 2024. They span a range of geographical regions, but Europe and the United States contributed the most publications. Empirical studies and simulation-based models dominated the research landscape (Sarr et al., 2024), using tools such as MATLAB, ray tracing, crop simulators, and irradiance models like PVLib and Sandia's Solar Positioning Algorithm (SPA) (Perna, 2021).

2.2. Key themes in the literature

2.2.1. PV impacts on light and microclimate

PV panels alter the surface energy balance by modifying direct and diffuse light availability (Najafabadi, 2024), which in turn affects photosynthetically active radiation (PAR), photo-synthesis, and microclimate variables such as temperature and humidity (Fagnano et al., 2024; Noor and Reeza, 2022). While some species adapt to shaded conditions through physiological responses like chlorophyll increase, shade-sensitive species may suffer from reduced yields or photoinhibition (Gupta et al., 2024).

Soil temperature and moisture are also affected (Chen et al., 2024). Shading can reduce evaporation and retain soil moisture (Feistel et al., 2022), which benefits dry climates but may create damp micro-environments prone to fungal diseases in humid regions (Hickey, 2023). Drip patterns from panels further influence soil wetting and microbial activity.

2.2.2. Modelling light distribution under PV systems

Modelling tools such as ray tracing, 3D irradiance mapping, and the Solar and Longwave Radiation Model (SLRM) are widely used to simulate ground-level light dynamics (Perna, 2021). Many models now account for both beam and diffuse light, especially important in bifacial PV systems (Sarr et al., 2024). Input parameters often include panel tilt, azimuth, geographic location, and cloud cover.

Recent models (Ko et al., 2023; Potenza et al., 2022) also incorporate crop-specific growth responses, such as those using GECROS or hybrid models that combine radiation physics with plant development simulations. These integrative approaches help bridge microclimate modification and ecological outcomes.

2.2.3. Vegetation suitability under PV systems

Leafy vegetables (e.g., lettuce, spinach) and fruiting crops (e.g., strawberries, to-matoes) are frequently found to perform well under partial shade, with improvements in quality or water use efficiency (Scarano et al., 2024). Ornamental species like Hydrangea also show positive growth. In contrast, high-light-demand crops such as maize and wheat tend to experience yield suppression in shaded zones (Gupta et al., 2024).

2.2.4. Light availability and photosynthetic efficiency

Photosynthetic Photon Flux Density (PPFD), expressed in $\mu mol/m^2/s$, is the key metric for assessing light availability for vegetation under PV arrays (RED Horticulture, 2023). Its variability across space and time under fixed-tilt installations creates micro-zones of differing light intensities, which can be strategically matched to crop types. Shade-tolerant C3 plants with low light compensation points (<200 $\mu mol/m^2/s$) are better suited for use beneath panels (Laub et al., 2022).

2.2.5. Ecological and land-use implications

Agrivoltaics may support ecosystem services such as biodiversity enhancement, erosion control, and extended growing seasons by mitigating environmental extremes. However, ecological risks include compaction, disrupted pollination, and altered habitat connectivity (Jedmowski et al., 2022). These trade-offs underscore the importance of careful spatial design and post-installation monitoring.

2.2.6. Gaps in current modelling practice

Despite growing model sophistication, several limitations persist. Many tools omit long-term ecological processes, hydrological interactions, or seasonal variability. Most are also calibrated for arid and Mediterranean climates, failing to fully capture the cloud cover, rainfall patterns, and diffuse light dominance typical of temperate climates like Aotearoa New Zealand. Furthermore, pasture-specific dynamics remain underexplored in the agrivoltaics literature.

2.3. Conclusion

The reviewed literature presents a growing body of evidence on how solar PV systems influence vegetation via light availability and microclimate regulation. However, existing models are often unsuited to temperate climates or long-term field conditions. This review supports the need for site-specific modelling frameworks that account for both irradiance variability and considers how much light different crops need to grow optimally under PV systems, particularly for pasture-based systems in regions such as Aotearoa New Zealand.

3. Research methods

This section provides an overview of the methods used to simulate ground-level solar irradiance under fixed-tilt photovoltaic (PV) arrays and assess the implications for vegetation. The research focussed on the Tauhei solar farm, a representative case study of large-scale solar deployment in Aotearoa New Zealand's Waikato region. Details of the 147 MW_{AC} project are provided in the resource consenting documentation (Environmental Protection Authority , 2022). The methodology draws on solar geometry, irradiance weather data, and shading simulation to calculate the light distribution beneath the PV panels. A mathematic Python-based modelling approach was used to estimate both beam and diffuse components of global irradiance, which were then converted into Photosynthetic Photon Flux Density (PPFD) to evaluate potential impacts on vegetation growth. This section further elaborates on the panel structure, solar position modelling, hourly irradiance data, and assumptions in the estimation of PPFD.

3.1. Research design

A simulation-based research design was employed, with the use of computational modelling tools to analyse solar radiation distribution under PV panels. This approach enabled a focused analysis of irradiance distribution using meteorological inputs and panel geometry. The aim was to develop a reproducible model that could be adapted for different spatial configurations and seasonal scenarios. The design also enabled the identification of irradiance gradients across the farm, which were then linked to potential vegetation outcomes.

The choice of a modelling-based method aligns with studies that favour predictive analysis when direct ecological observation is constrained (Potenza et al., 2022). It also facilitates scenario-based testing of light availability across time and space, enabling a virtual assessment of microclimatic effects across the landscape. Furthermore, it provides a means to examine long-term annual variability and its seasonal characteristics, which would otherwise be challenging to monitor empirically.
The study aimed to (i) simulate the spatial distribution of solar radiation beneath fixed-tilt PV panels at Tauhei solar farm; (ii) compute the shading factors affecting direct and diffuse components of irradiance using Python; (iii) estimate PPFD at ground level and interpret its implications for vegetation suitability based on published light thresholds; and (iv) examine seasonal variations in ground-level irradiance and assess zones of persistent shading and light availability.

3.2. Case study: Tauhei solar farm, Waikato

The case study site is Tauhei solar farm, located in the Waikato region of Aotearoa New Zealand. The site spans 182 hectares and is expected to generate 280 GWh annually with a 200 MW fixed-tilt bifacial PV system (SLR Consulting, 2024). Although it is converting dairy farming, sheep grazing is maintained on the land, which highlights its dual-use nature. This farm was selected because it reflects the emerging agrivoltaic landscape in Aotearoa New Zealand and provides a realistic template for future developments. Its consistent tilt and uniform layout make it ideal for spatially explicit modelling of solar irradiance.

The farm's selection was also influenced by its representative environmental conditions typical of the North Island's central zone. These characteristics make Tauhei a suitable pilot for understanding how fixed-tilt PV systems might influence ecological processes across similar landscapes. Its accessibility and relevance to future policy decisions on land co-use made it an ideal research site.

3.3. Modelling approach

The modelling was conducted using Python, leveraging packages for solar geometry, trigonometric projection, and geospatial analysis. The approach simulates the movement of the sun across the sky and projects the resulting shadows cast by the PV panels onto a fixed ground study area. The calculations account for solar zenith and azimuth angles, panel tilt, and orientation. The shadow polygons are clipped against the ground area and used to derive shading factors for each hour of the year.

The simulation process was broken into key stages: (1) establishing the solar position; (2) generating panel geometry; (3) simulating shadow projection; and (4) calculating irradiance loss within the study area.

3.4. System parameters

3.4.1. Assumptions

- Panels are opaque and block all direct beam radiation beneath their structure.
- Diffuse irradiance is assumed to be isotropic (evenly distributed across the sky dome).
- Ground reflectance and albedo effects are ignored.
- Soil and vegetation characteristics are assumed to be uniform throughout the study area.

3.4.2. Solar array technical specifications

As illustrated in Figure 1, the solar arrays have the following technical specifications:

- Array width: 4,530 mm
- Array length (row length): 14,970 mm
- Panel tilt angle (β): 20°
- Lowest panel edge height (Hpanel): 900 mm
- Highest panel edge height (Hpanel, top): 2,600 mm
- Row Spacing (pitch): 3,250 mm

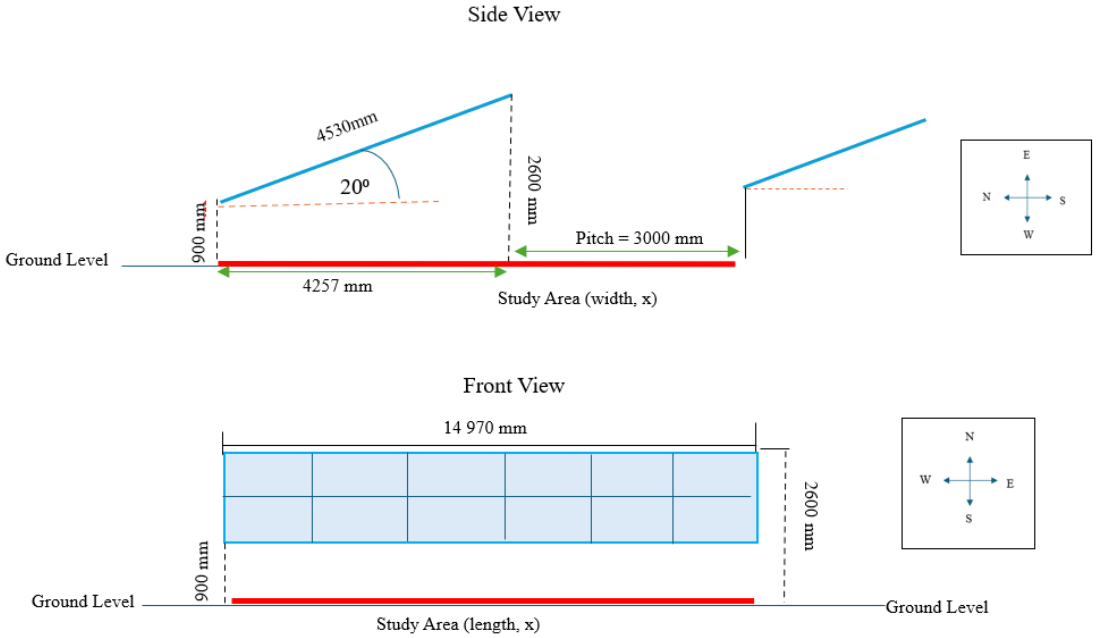

Figure 1. Solar panel array and study area

3.4.3. Panel geometry and study area

The zenith angle (Z) and azimuth angle (γs) of the sun were computed for each hour. The study area was defined beneath a single row of panels with dimensions 14.97 m (length) x 7.257 m (width), representing the horizontal ground shadow zone, with the following parameters:

- Panel height (Hpanel): Distance from ground to the lowest panel edge.
- Panel tilt (β): Angle between the panel surface and horizontal.
- Solar zenith angle (Z): Angle between the sun and the vertical.
- Solar azimuth angle (γs): Direction of the sun's position.
- Panel azimuth angle (γp): Orientation of the panel.

3.5. Irradiance modelling and shading factors

The total global irradiation is given by:

$$G_{total} = DNI + DHI \quad (1)$$

Where G_{total} is the Global Horizontal Irradiation (GHI), DNI is the Direct Normal Irradiance, or beam irradiance, and DHI is the Diffuse Horizontal Irradiance.

3.5.1. Direct beam (direct normal) irradiance and direct beam shading factor

Beam irradiance (direct irradiance) is the component of sunlight that travels unimpeded in a straight line from the sun to the Earth's surface, unaffected by atmospheric scattering. It is calculated for tilted surfaces (e.g., solar panels) using solar geometry and atmospheric conditions, as defined by the angle of incidence (Quaschning and Hanitsch, 1995):

$$I_t = I \cdot max(0, \frac{cos(\theta)}{sin(\alpha_s)}) \quad (2)$$

Where I is the horizontal direct irradiance, θ is the angle of incidence, and α_s is the solar altitude.

The beam shading factor quantifies the reduction in beam irradiance due to obstructions (in this case, PV panels). The beam shading factor, fb, is the shading factor for the beam irradiance and is given by:

$$fb = \frac{A_{total}}{A_{shaded}} \quad (3)$$

Where fb is the shading factor, A_{shaded} is the shaded area on the ground, and A_{total} is the total fixed ground area considered.

This shading results in a reduction of solar irradiance reaching the ground. The irradiance loss is thus captured by adjusting the ground-level global irradiance GHI_{ground} based on the shaded fractions of both direct and diffuse radiation. This is expressed as:

$$GHI_{ground} = DNI\ (1 - fb) + DHI\ (1 - fd) \quad (4)$$

Therefore, (1-fb) is the fraction of the ground that is exposed to direct beam irradiance (see Figure 2).

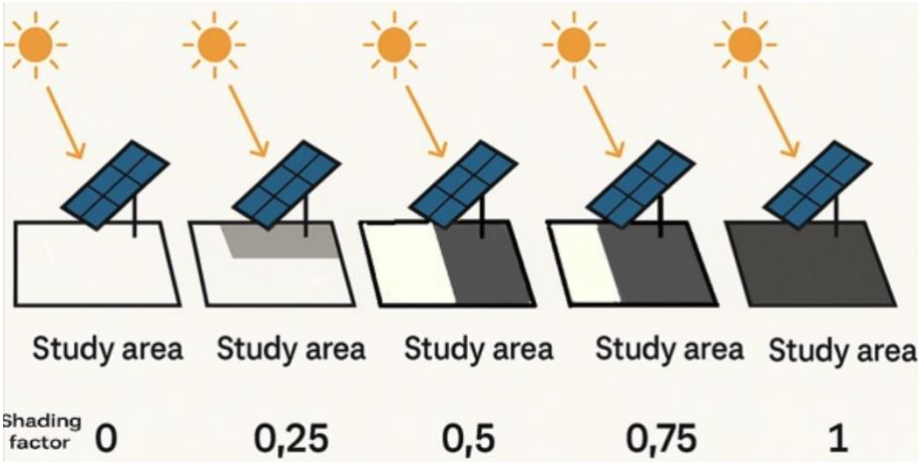

Figure 2. Shading factor illustration
(Source: OpenAI, 2024)

3.5.2. Diffuse irradiance

Diffuse irradiance is the component of sunlight scattered by atmospheric particles, clouds, and molecules, reaching the Earth's surface indirectly from all directions of the sky hemisphere rather than in a direct beam. This contrasts with direct irradiance and contributes to solar energy systems, especially under cloudy conditions or partial shading (Quaschning and Hanitsch, 1995; Perez et al., 1987). The Diffuse Shading Factor quantifies the fraction of diffuse solar radiation blocked by the solar panels, affecting the amount of diffuse irradiance that reaches the ground beneath them. According to Essery and Marks (2007) the amount of diffuse radiation that reaches a surface is intricately connected to the portion of the sky dome visible from that surface. This relationship is influenced by several factors, including the angular distribution of diffuse radiation, topographic features, and atmospheric components.

Mapping diffuse solar radiation involves understanding its distribution across the sky hemisphere, which is affected by various atmospheric and environmental conditions. A technique involving all-sky photographs can be used to create a map of diffuse solar radiation. This method utilizes the correlation between digitized photographs and direct radiance measurements, helping to determine the radiance for different densities across the sky dome (Mcarthur and Hay, 1981).

In regions with complex topographies, the distribution of diffuse solar radiation is not uniform. Factors like slope, aspect, shadows, and sky obstruction play significant roles. Parametrizations developed to assess clear-sky solar radiation in such regions consider these variables, allowing for accurate modelling of solar radiation, including both direct and diffuse components (Essery and Marks, 2007). The interplay between diffuse and direct beam radiation is also crucial for terrestrial ecosystems, as these two types of radiation impact processes like photosynthesis differently. Diffuse radiation often results in higher efficiencies in light use by plant canopies and reduces the likelihood of photosynthetic saturation when compared to direct radiation. This difference in efficiency underscores the importance of diffuse radiation in areas where plants are the primary photosynthesizers (Gu et al., 2002).

The diffuse radiation reaching the Earth's surface is influenced by atmospheric aerosols and clouds. These elements modulate the proportion of diffuse to direct radiation, impacting the total solar energy received at the surface. In conditions with high aerosol

concentrations, there is typically an increase in diffuse radiation as aerosols scatter the solar beams (Xia, 2014). While diffuse radiation is affected by atmospheric components, it is important to consider its role in environments with different optical properties, such as urban areas versus rural landscapes. Urbanized areas, with their complex geometries, can witness significant variations in diffuse radiation due to reflections and obstructions caused by buildings and streets (Oke, 1982).

Overall, understanding how much diffuse radiation reaches a specific surface requires a comprehensive approach that considers the visible portion of the sky dome, topographic influences, atmospheric conditions, and geographical location. Each of these factors contributes to the dynamic nature of diffuse solar radiation distribution. The sky diffuse irradiance is, therefore, substantially affected by the radiance levels and distributions over the sky in the direction viewed from the surface. An appropriate way of determining the sky diffuse irradiance on an inclined plane would be to integrate the radiance over the sky dome visible to the surface.

The diffuse irradiance, $I_{\beta d}$ can be determined as:

$$I_{\beta d} = \iint R_{\alpha\gamma} cos\theta \ (sin\alpha cos\beta + \cos\alpha sin\beta cos\gamma \ ) \ d\gamma d\alpha \tag{5}$$

Where $R_{\alpha\gamma}$ is the radiance of sky element at altitude θ and azimuth γ, and β is the inclination angle of sloped surface (Danny and Li, 2004). This formula requires the sky diffuse component to be divided into n by m angular zones to simplify the equation for numerical computation (Danny and Li, 2004).

3.5.3. Diffuse shading factor

The shading factor for diffuse radiation, f_d represents the fraction of the sky hemisphere obscured by obstacles. It is derived by comparing the irradiance contributions from visible and obstructed sky segments (Quaschning and Hanitsch, 1995):

$$fd \ = \frac{\int_{\alpha=0}^{\pi/2} \int_{\alpha=0}^{2\pi} f_b(\alpha,\gamma) R_{\alpha\gamma} \cos(\beta) d\Omega}{\int_{\alpha=0}^{\pi/2} \int_{\alpha=0}^{2\pi} R_{\alpha\gamma} \cos(\beta) d\Omega} \tag{6}$$

Assuming isotropic radiance, i.e. $R_{\alpha\gamma}$ is a constant, the double integral can be discretized into n×m angular segments for numerical approximation (Najafabadi, 2024):

$$fd \ = \frac{\sum_{i=1}^{n} \sum_{j=1}^{m} f_{b,ij}(\alpha_i, \gamma_j) cos(\beta_{ij}) \cos(\alpha_i) \Delta\alpha\Delta\gamma}{\sum_{i=1}^{n} \sum_{j=1}^{m} cos(\beta_{ij}) \cos(\alpha_i) \Delta\alpha\Delta\gamma} \tag{7}$$

For horizontal surfaces, this simplifies further to:

$$fd \ = \frac{\sum_{i=1}^{n} \sum_{j=1}^{m} f_{b,ij}(\alpha_i, \gamma_j) sin(\alpha_i) \cos(\alpha_i)}{\sum_{i=1}^{n} \sum_{j=1}^{m} sin(\alpha_i) \cos(\alpha_i)} \tag{8}$$

Empirical studies (Perez et al., 1987) show that diffuse shading losses are often <5% in unshaded environments. For the sake of simplification and avoiding computational intensiveness for modelling the diffuse shading factor, fd ,this model assumes the diffuse

radiation loss to be negligeable, (1-fd)≈0, thus the ground irradiation (equation 4) is simplified to:

$$GHI_{ground} = DNI \cdot (1 - fb) + DHI \quad (9)$$

3.6. Simulation and analysis: The model

3.6.1. Shadow projection beneath the PV panels

This method follows the shading model of Quaschning and Hanitsch (1995) and accounts for the sun's position. It uses panel geometry to project the shadow of and object in the path of the sun light. The panel was modelled as a 3D polygon, and its shadow projection was computed by intersecting solar rays (from the sun direction vector) with the ground plane (z = 0). Each vertex of the panel was projected individually, and the resulting shadow polygon was formed. The shaded area was then 'clipped' using the boundaries provided by the study area using the Shoelace formula.

A global coordinate system relative to the solar panel and its position was established, as follows :

- x-axis: East-West direction;
- y-axis: North-South direction; and
- z-axis: Vertical (upward).

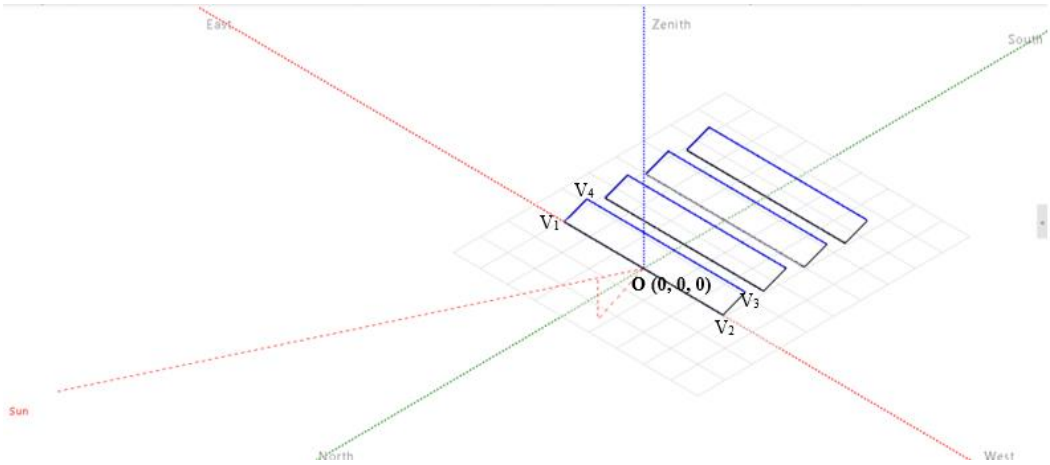

Figure 3. Representation of the panel array using geographic reference

Each corner of the panel is a vertices point in the coordinate system. The vertices are the matrices that form the basis of the projection calculations. The origin point is at (0,0,0), which is suspended on the northern most edge of the panel at the centre point (see Figure 3). Similarly, the projected shadow forms a polygon on the ground with its own vertices:

$$v_i = (x_i, y_i, z_i) \quad (10)$$

With: v_1 = (-7.284 ,0,0.9)
v_2 = (7.284 ,0,0.9)
v_3 = (7.284 ,7.257,2.6)
v_4 = (-7.284 ,7.257,2.6)

The sun direction vector is determined from the following:

$$s = \begin{bmatrix} \cos(\gamma)\cos(\alpha) \\ \sin(\gamma)\cos(\alpha) \\ sin(\alpha) \end{bmatrix} \quad (11)$$

Where α is the sun's altitude, and γ is the sun's azimuth.

For each vertex, v_i, the shadow is cast in the opposite direction of the sun rays (-s). Its shadow on the ground (z = 0) is calculated by projecting along -s:

$$\begin{cases} x = x_i - t cos\gamma cos\alpha \\ y = y_i - t sin\gamma cos\alpha \\ z = z_i - t sin\alpha \end{cases} \quad (12)$$

Where $t=z_i/(\sin(\alpha))$ is the gradient defining the distance along the shadow's path (straight line) along -s to reach the ground, i.e. when z= 0.

The horizontal displacement is determined by: $\Delta x = t\cos(\gamma)\cos(\alpha)$; $\Delta y = t\sin(\gamma)\cos(\alpha)$. Simplifying the shadow equation using $\tan(\alpha)=\sin(\alpha)/\cos(\alpha)$, the coordinates to the shadow cast, or projected by each vertex, v_i, becomes:

$$x_{shadow,i} = x_i - \frac{z_i}{tan(\alpha)} \quad sin(\gamma) \quad (13)$$

$$y_{shadow,i} = y_i - \frac{z_i}{tan(\alpha)} \quad cos(\gamma) \quad (14)$$

These coordinates form the shadow vertices s_1, s_2, s_3, s_4, which will form the shadow polygon on the ground.

Recalling that the study area is a rectangle on the ground (in meters):
$-7.485 \leq x \leq 7.485$; $0 \leq y \leq 7.257$

The shaded area is then clipped within the limits of the study area. For the clipped polygon, the area is computed using the shoelace formula (Quaschning and Hanitsch, 1995):

$$A_{shaded} = 0.5 * \left| \sum_{i=1}^{n} (x_i\, y_{i+1} - x_{i+1}\, y_i) \right| \quad (15)$$

The beam shading factors, given by equation 3, can now be estimated using the shaded study area and the total study area.

3.6.2. Data source and preprocessing

Hourly meteorological data for 2018 calendar year was used, which was obtained from SolarGIS for the Waikato region. These were provided in a .csv format in European time zone. The dataset included GHI, DNI, and DHI, along with solar position angles. Date and time components were merged into a single datetime index in Python and converted to

the Pacific/Auckland time zone. The data were cleaned for daylight saving anomalies and tested for continuity in hourly time steps; no missing values were present.

3.6.3. Estimating ground irradiance, GHIground, in the study area

The shading factors were computed producing a table of beam shading factors and a constant estimation of diffuse shading factor (isotropic sky model assumption). The ground irradiance values were then calculated as follows:

$$GHI_{ground} = DNI_{shaded}\, cos(zenith) + DHI \quad (16)$$

Where: DNI_{shaded}=DNI×(1-shading_factor), and DHI_{shaded}=DHI, i.e. ($1\text{-diffuse}_{shading\_factor}$) ≈0.

3.6.4. Estimating Photosynthetic Photon Flux Density (PPFD)

PPFD was estimated from the shaded GHI using a conversion factor of 2.02 µmol/J (i.e., 1 $W/m^2 \approx 2.02$ µmol/m^2/s), following established methods for full-spectrum sunlight under clear sky conditions (Bosch et al., 2009). This allowed for direct ecological interpretation of irradiance levels. A spatial PPFD map was generated for each season, using seasonal hourly averages to highlight areas with light limitations for common pasture and crop types.

3.6.5. Seasonal comparisons via solstices and equinoxes

To understand seasonal effects on PPFD and GHI values, the following representative dates were selected:

- Summer solstice (December 21);
- Winter solstice (June 21);
- Spring equinox (September 22); and
- Autumn equinox (March 21).

These seasonal samples will help quantify differences in radiation availability and shading patterns, and their impact on plant growth under PV panels.

3.6.6. Irradiance heat maps

Using Python's Matplotlib and GeoPandas, irradiance heat maps were generated for each season, visually representing the spatial distribution of light under the panels. These maps were used to interpret PPFD gradients and identify zones with sufficient light for vegetation growth.

All of the Python coding is provided in the supplementary material.

3.7. Limitations

Several limitations of the study are acknowledged. First, the research does not include real-world validation via in-situ sensors. Also, the impact of panel reflectivity and albedo changes were omitted. Soil and vegetation feedback mechanisms, such as evapotranspiration, moisture retention, and so forth, were not dynamically simulated, and the ground conditions were assumed to be sufficient for pasture growth.

4. Results

This section presents and analyses the outcomes of the irradiance and shading simulations for the Tauhei Solar Farm. The focus is on evaluating seasonal patterns of ground-level irradiance, shading intensity, and the spatial distribution of Photosynthetic Photon Flux Density (PPFD) under the fixed-tilt PV panels. The section also explores the

practical implications of the results, both for vegetation management and land-use optimisation in agrivoltaic systems.

4.1. Beam shading factors

The shadow polygon that was formed by projecting panel vertices and clipping them within a fixed ground study area under the panel are summarised in Table 1. The table represents how much of the direct beam sunlight (DNI) is blocked by the panel array at the ground level. The shading factors have a value typically between 0 and 1, where, as per Figure 2:

- 1 means full shading (no direct beam reaching the ground); and
- 0 means no shading (full direct beam reaches ground).

Table 1. Beam, or direct, irradiance shading factors

Azimuth (deg)	-180	-160	-140	-120	-100	-80	-60	-40	-20	0	20	40	60	80	100	120	140	160	180
Elevation (deg)																			
90	0.587	0.587	0.587	0.587	0.587	0.587	0.587	0.587	0.587	0.587	0.587	0.587	0.587	0.587	0.587	0.587	0.587	0.587	0.587
80	0.628	0.621	0.61	0.596	0.582	0.564	0.545	0.531	0.523	0.523	0.523	0.531	0.545	0.564	0.582	0.596	0.61	0.621	0.628
70	0.672	0.657	0.634	0.606	0.576	0.54	0.502	0.473	0.457	0.456	0.457	0.473	0.502	0.54	0.576	0.606	0.634	0.657	0.672
60	0.722	0.697	0.66	0.616	0.57	0.514	0.454	0.409	0.383	0.38	0.383	0.409	0.454	0.514	0.57	0.616	0.66	0.697	0.722
50	0.783	0.745	0.691	0.627	0.561	0.482	0.397	0.332	0.293	0.286	0.293	0.332	0.397	0.482	0.561	0.627	0.691	0.745	0.783
40	0.852	0.808	0.729	0.639	0.548	0.441	0.324	0.233	0.175	0.16	0.175	0.233	0.324	0.441	0.548	0.639	0.729	0.808	0.852
30	0.785	0.748	0.73	0.651	0.526	0.38	0.221	0.093	0.003	0	0.003	0.093	0.221	0.38	0.526	0.651	0.73	0.748	0.785
20	0.659	0.621	0.61	0.609	0.477	0.276	0.06	0	0	0	0	0	0.06	0.276	0.477	0.609	0.61	0.621	0.659
10	0.297	0.293	0.333	0.363	0.284	0.056	0	0	0	0	0	0	0	0.056	0.284	0.363	0.333	0.293	0.297
0	1	1	1	1	1	1	1	1	1	1	1	1	1	1	1	1	1	1	1

4.2. Model results for the Global Ground Irradiance

4.2.1. Day visualisation of the equinoxes and solstices

Figure 4 presents the daylight profile of global horizontal irradiance on the ground (GHIground) across the four representative days of the year, which corresponds to the two solstices and two equinoxes. The values represent irradiance measured beneath the PV arrays, accounting for shading losses due to the fixed-tilt configuration.

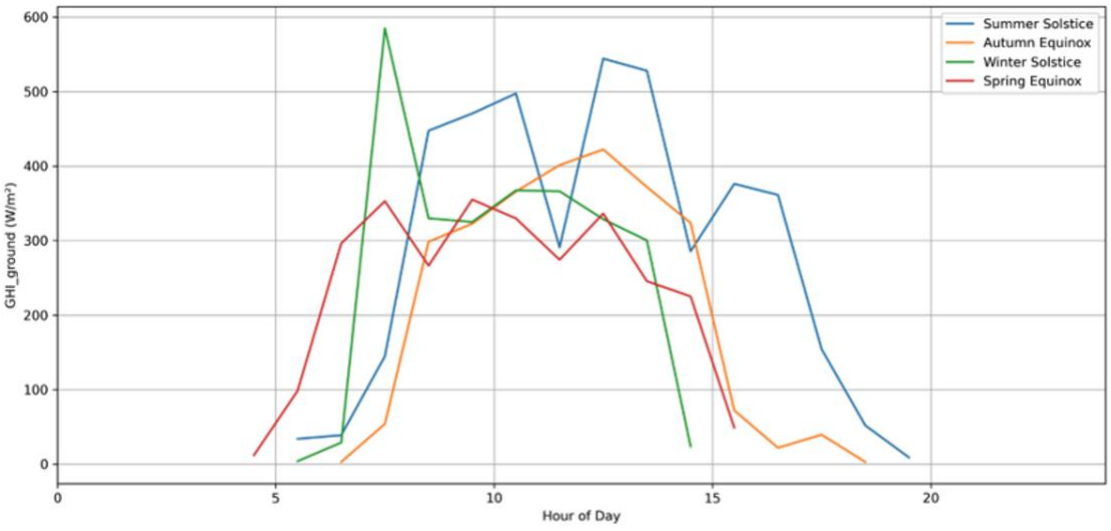

Figure 4. Day visualisation of the Equinoxes and Solstices

The summer solstice (blue line) shows the highest and most sustained irradiance, peaking at over 550 W/m^2 around midday. The winter solstice (green line) shows the sharpest decline in irradiance duration and peak values, with a maximum around 330 W/m^2. The equinoxes (red for spring, orange for autumn) lie between the two extremes, with the autumn profile showing a slightly higher and more sustained peak compared to spring.

Figure 5 illustrates the ground-level global horizontal irradiance across the four representative seasonal days, with each subplot comparing the original irradiance values (blue line) to their smoothed counterparts (orange dashed line) using a rolling average filter. The rolling average line helps clarify underlying seasonal trends by filtering out short-term variability in irradiance, possibly due to shifting shadows, cloud cover intermittency, or sensor variability.

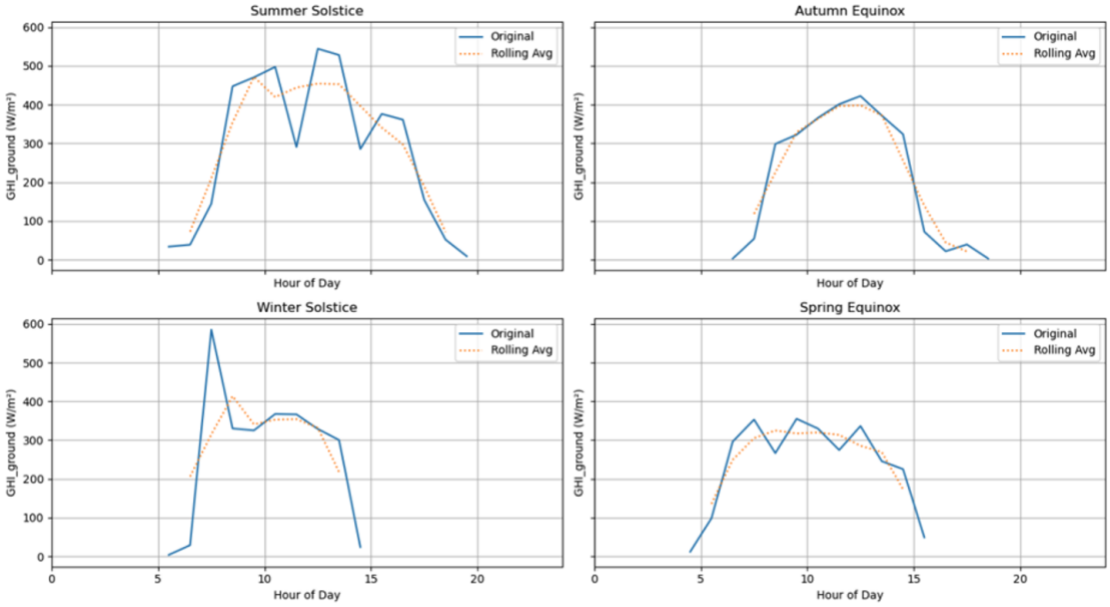

Figure 5. GHIground rolling average for the four representative days

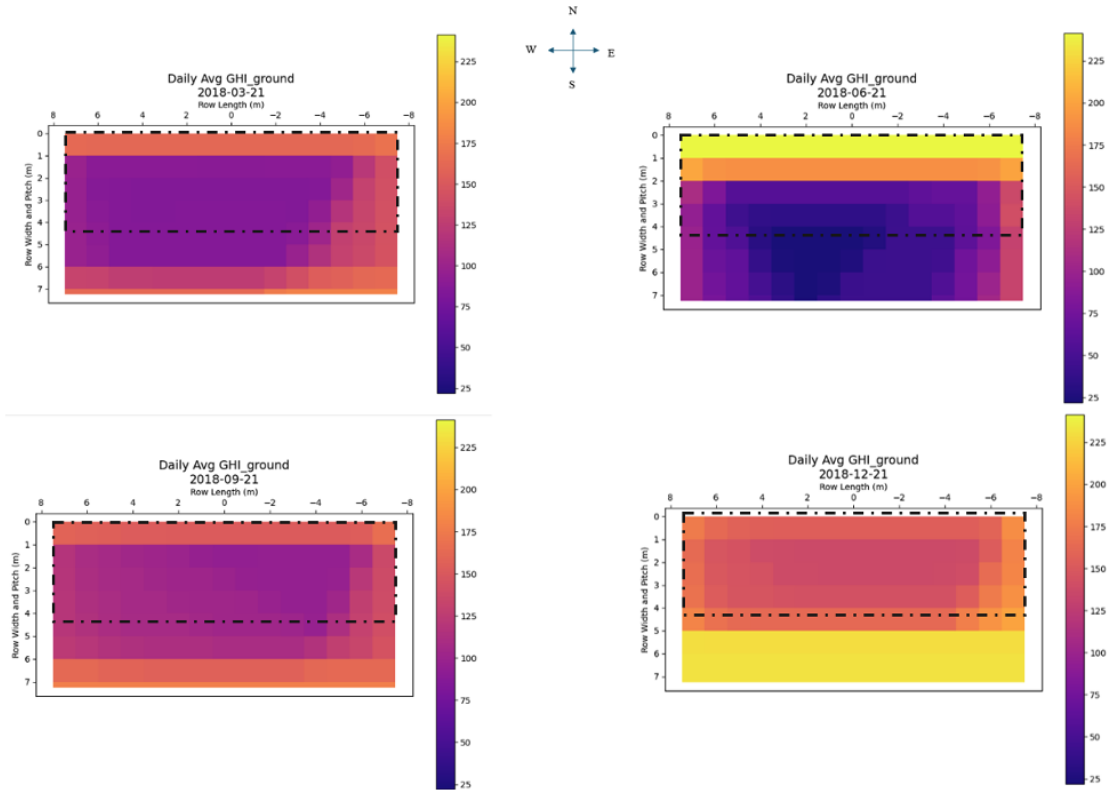

Figure 6. Spatial heat maps for ground irradiance for the representative seasons

4.2.2. Spatial heat maps for ground irradiance

Figure 6 presents the spatial heat maps of daily average global horizontal irradiance at ground level beneath the PV array for the four key solar calendar days: the two equinoxes (March 21 and September 21) and the two solstices (June 21 and December 21).

The March and September equinoxes display near-symmetrical shading gradients. The central area beneath the panels receives lower irradiance (50–125 W/m^2), with increasing intensity toward the panel edges. The June solstice shows the most pronounced central shading, with GHIground dropping below 50 W/m^2 directly beneath the panel. The northern edge receives much unshaded exposure. The December solstice exhibits an inverse pattern, with higher irradiance centrally (>175 W/m^2 on average) and a more uniform spatial distribution.

4.2.3. Comparison between solar resource and GHIground

Figure 7 compares the true seasonal average global horizontal irradiance (GHI) and corresponding ground-level irradiance (GHIground) for each of the four meteorological seasons. Summer and Spring exhibit the highest GHI values, each averaging above 340 W/m^2, with GHIground showing a ~15% reduction due to shading. Autumn and Winter display lower seasonal irradiance overall, though the relative difference between GHI and GHIground is smallest in winter.

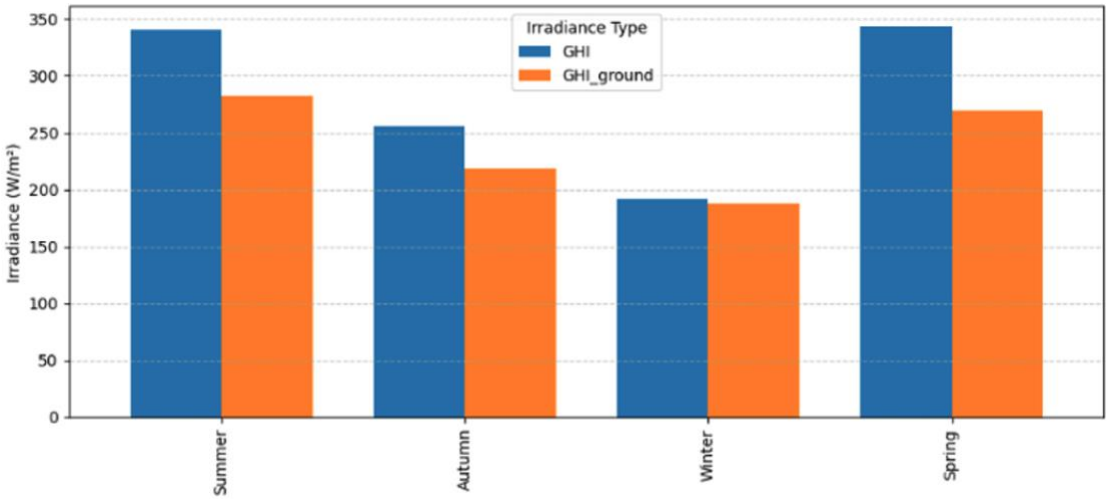

Figure 7. Comparison of seasonal average GHI and the average of ground irradiance

4.3. The model results for the Photosynthetic Photon Flux Density (PPFD)

4.3.1. Daily average PPFD across the seasonal cycle

Figure 8 illustrates the modelled daily average PPFD beneath the PV array over a full calendar year (2018). Values are highest during summer and spring, often exceeding 700 $\mu mol/m^2/s$. Autumn shows moderate levels (400–600 $\mu mol/m^2/s$), while winter presents the lowest PPFD, frequently falling below 400 $\mu mol/m^2/s$.

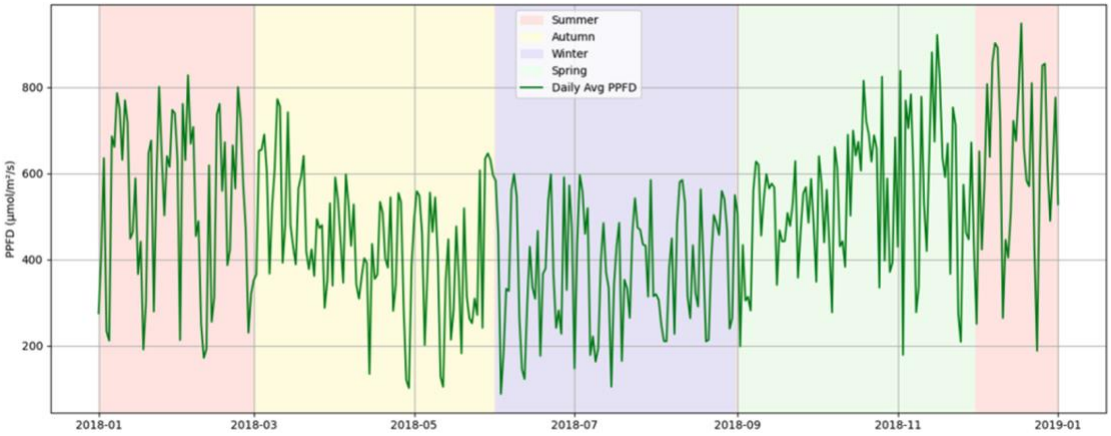

Figure 8. Daily average PPFD across the seasonal cycle

4.3.2. Spatial distribution of daily average PPFD across seasons

Figure 9 shows the heat maps of daily average PPFD beneath the PV array for four key dates representing each season. In the autumn and spring equinoxes there are balanced and moderately high PPFD values (200–350 μmol/m^2/s). The summer solstice demonstrates the highest under-panel PPFD with values reaching close to 400 μmol/m^2/s. Winter solstice exhibits the most severe shading, with the central under-panel region receiving as little as 50–100 μmol/m^2/s.

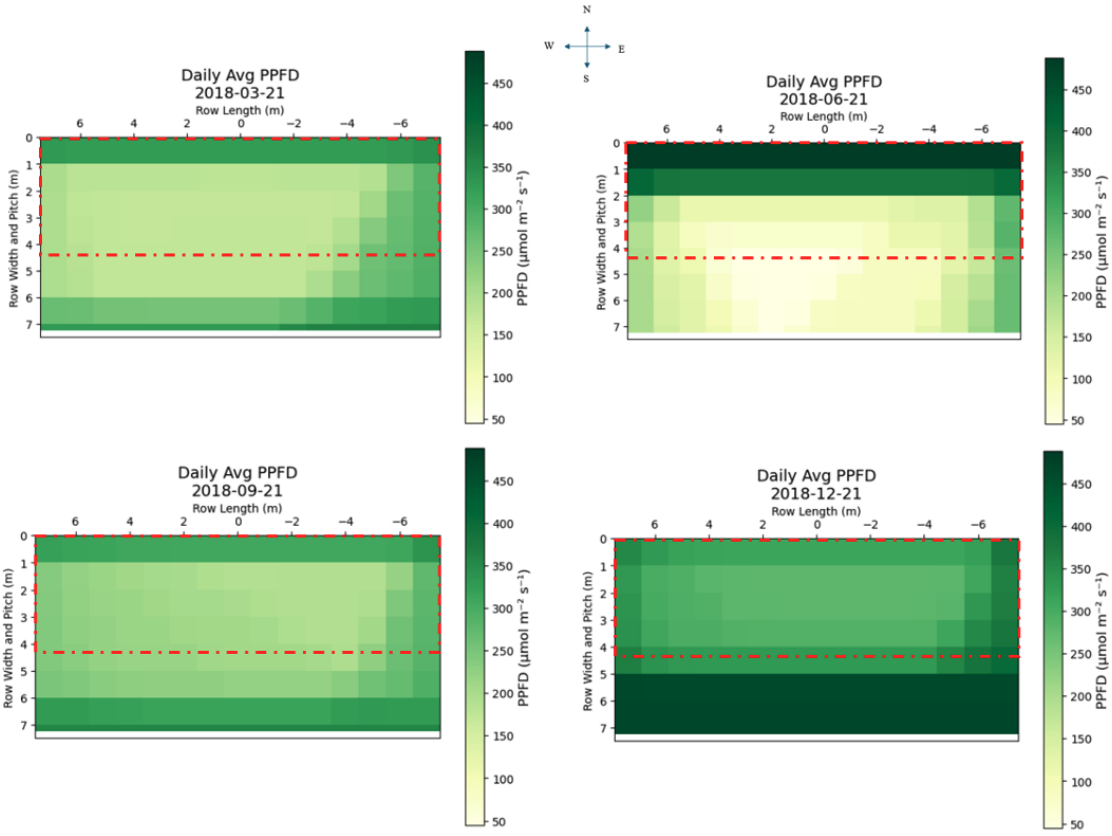

Figure 9. Heat map of PPFD across seasons (representative days)

4.3.3. Seasonal average PPFD across the study area

Figure 10 illustrates the seasonal average PPFD in the PV array. The values are based on daily mean PPFD readings integrated over each season, showing cumulative light availability for vegetation growth.

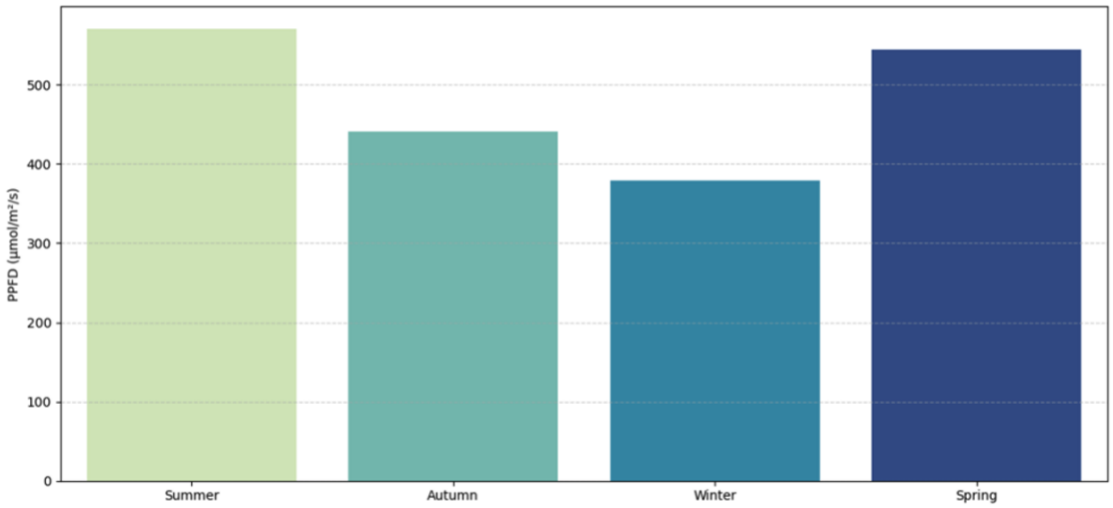

Figure 10. Seasonal PPFD averages

4.4. Summary of averaged ground irradiance and PPFD results by season

To contextualise light availability for vegetation beneath the PV panels, seasonal averages of both global horizontal irradiance at ground level and the corresponding PPFD are summarised in Table 2. These values were derived from the full seasonal datasets and provide a high-level comparison of the solar energy resource and biologically active light across the year.

Table 2. Summary of average of season ground irradiance and average PPFD

Season	Average Ground GHI (W/m2)	Average PPFD (umol/m²/s²)
Autumn	218.3	440.96
Spring	269.71	544.81
Summer	282.21	570.06
Winter	187.65	379.06

4.5. Vegetation suitability under light conditions

To assess the potential for integrating vegetation beneath the PV arrays, Table 3 presents a filtered subset of plant species that align with the observed average PPFD values recorded in the study area. A more complete list of species and PPFD values are provided in the supplementary material. The selected crops demonstrate PPFD requirements within the 200–800 µmol/m^2/s range, aligning with the average under-panel PPFD observed during spring and summer.

There is a varying range in PPFDs of the vegetation. Nonetheless, these species represent viable candidates for agronomic experimentation in specific irradiance zones beneath the array. However, it is important to note that light availability during winter drops significantly below their active growth thresholds. This raises concerns about year-round viability of the vegetation. The perennial ryegrass (Lolium perenne L.) is the most widely sown grass type in Aotearoa New Zealand as well as in the Waikato regions as it grows in a variety of condition and is easy to manage. According to Brito et al. (2023), cultivating

this grass under 400 µmol m^{-2} s^{-1} light intensity supports peak dry biomass yield, if water and energy inputs are sufficient.

Table 3. Plants with the necessary PPFD required to grow within the study area

Plant	Genus	PPFD (µmol/m^2/s)	DLI (mol/m^2/d)
Blackberry	Rubus	200 – 300	8 – 14
Chrysanthemums	Chrysanthemum	200 – 300	10 – 14
Mint	Mentha	200 – 400	10 – 20
Parsley	Petroselinum crispum	200 – 400	10 – 20
Sage	Salvia officinalis	200 – 400	10 – 20
Garden Lettuce	Lactuca	250 – 350	14 – 16
Roses	Rosa	350 – 450	18 – 22
Tomatoes	Solanum lycopersicum	350 – 800	22 – 30
Strawberry	Fragaria	400 – 600	17 – 28

Table 4 presents the seasonal light requirements (DLI and PPFD) for a range of turfgrass cultivars, adapted from Unruh (2015). These values offer a reference for evaluating grass species beyond perennial ryegrass that may be suited for agrivoltaic environments or alternative grazing zones across the study area.

Table 4. Daily light requirements for grass species

Turfgrass Cultivar	Summer		Winter		Spring	
	DLI (mol/m²/day)	PPFD (micr-mol/m²/s²)	DLI (mol/m²/day)	PPFD (micr-mol/m²/s²)	DLI (mol/m²/day)	PPFD (micr-mol/m²/s²)
Tifway hybrid bermudagrass	21	486.11	10.6	245.37	17.9	414.35
TifGrand hybrid bermudagrass	19.9	460.65	9.8	226.85	14.6	337.96
Celebration common bermudagrass	19.6	453.70	8.8	203.70	14.9	344.91
TifBlair centipedegrass	13.4	310.19	9.5	219.91	14.1	326.39
Floratam St. Augustinegrass	11.8	273.15	8.5	196.76	11.6	268.52
Palisades zoysiagrass (japonica)	11.2	259.26	8.2	189.81	11.2	259.26
Captiva St. Augustinegrass	10.9	252.31	8	185.19	11.5	266.20
BA-417 zoysiagrass (matrella)	10.8	250.00	7.3	168.98	10.6	245.37
JaMur zoysiagrass (japonica)	10.3	238.43	6.8	157.41	10.5	243.06

(Source: Unruh, 2015)

5. Discussion

This section interprets the findings from the irradiance and PPFD simulations conducted at the Tauhei Solar Farm. It focuses on their implications for agrivoltaic viability, considering seasonal and spatial dynamics, and the broader literature. The discussion is structured around the main research question: How does a fixed-tilt PV system affect ground-level light availability and vegetation growth potential?

5.1. Seasonal trends and shading dynamics

The simulations confirmed that seasonal variations in GHIground and PPFD are pronounced, with summer and spring providing the highest levels of irradiance and winter the lowest. This reflects expected variations in solar altitude and day length. Rolling average profiles further highlight the influence of atmospheric variability, where smoother irradiance patterns suggest clearer conditions during autumn compared to spring.

During summer, sustained irradiance exceeding 550 W/m^2 and daily PPFD above 700 µmol/m^2/s supports the active growth of light-demanding vegetation (Weselek et al., 2019). In contrast, winter PPFD values often fall below 400 µmol/m^2/s, approaching or falling beneath compensation points for many C3 crops (Laub et al., 2022), thereby constraining productivity.

5.2. Spatial light distribution and ground-level variability

The heat maps show non-uniform irradiance distribution caused by the panel array. Winter (June) shadows extend centrally with irradiance <50 W/m^2 under the panels, while summer displays more uniform light penetration with GHIground >175 W/m^2 in many areas. These spatial contrasts arise from seasonal solar geometries, particularly lower solar angles in winter.

Edge zones receive consistently higher irradiance due to grazing-angle radiation. These heterogeneities mirror the zone-based shading patterns identified by Adeh et al. (2018). Intermediate shading in spring and autumn reflects transitional solar paths and turbidity effects (Danny and Li, 2004).

This spatial-temporal variation suggests a need for diverse planting strategies that match vegetation types with irradiance availability.

5.3. Interpretation of seasonal PPFD values and GHI reduction

Seasonal GHIground is consistently lower than total GHI due to shading. The greatest relative reduction is observed in spring, followed by summer and autumn. Winter displays a small GHI-GHIground difference due to already limited solar input, indicating ambient solar constraints are more limiting than shading during that season.

Seasonal PPFD shows biologically significant variation. Summer levels >600 µmol/m^2/s support crop and forage viability. In spring and autumn, 400–600 µmol/m^2/s is sufficient for moderate-light crops. Winter PPFD <300 µmol/m^2/s precludes active growth for most species.

These results affirm that seasonal and spatial dynamics of light under fixed-tilt systems require zone-specific and seasonally adaptive strategies. In summer, shading may offer protection from heat stress (Marrou et al., 2013), while winter necessitates dormancy or soil conservation approaches.

5.4. Crop suitability based on PPFD thresholds

The results confirm that moderate-light crops like lettuce, parsley, mint, sage, and cilantro are viable in spring and autumn under PPFD levels of 300–600 µmol/m^2/s. These species tolerate partial shade and are commonly used in agrivoltaic trials. Garden lettuce and mint, especially, are well-suited to semi-shaded conditions.

Strawberries are highlighted for their seasonality: active growth aligns with spring/summer light, while winter dormancy avoids light limitations. High-light crops like tomatoes and roses (>600 µmol/m^2/s) are feasible only in high-irradiance zones, such as inter-row corridors (Potenza et al., 2022). Maize and sunflowers require over 800 µmol/m^2/s and thus fall outside viability.

Perennial ryegrass, a key forage species in Aotearoa New Zealand, tolerates ~400 µmol/m^2/s (Brito et al., 2023) but may require input support. Low-light turfgrass options such as BA-417 zoysiagrass, TifBlair centipedegrass, and Captiva St. Augustinegrass can maintain year-round cover under shade.

These findings validate a tiered land-use model using light-tolerant species for under-panel zones, moderate-light species for edge areas, and dormant or conservation species in winter.

5.5. Limitations, and policy relevance

This study's modelling relies on simulated solar geometry and shadow projection rather than ground-based validation. While outputs align with existing literature (Scarano et al., 2024; Potenza et al., 2022), use of in-situ sensors in future work would enhance accuracy. Intra-seasonal weather anomalies were not modelled, and species suitability was assessed from literature rather than trial data. The use of uniform sky models also excluded dynamic interactions like albedo feedback (Vignola et al., 2021).

Socio-economic and policy considerations, including landholder engagement, were beyond the scope but remain essential for real-world adoption (Brent, 2024; Hernandez et al., 2014).

6. Conclusions

The study concludes that the fixed-tilt PV arrays at Tauhei modify ground-level PPFD both seasonally and spatially. Most of the year, under-panel zones are low-light, with high irradiance limited to edges and summer periods. Crop suitability depends on aligning physiological light needs with seasonal patterns. Low-light turfgrass and dormant crops such as strawberries present year-round options.

Winter shows the least irradiance but also the smallest GHI-GHIground difference, suggesting that PV shading has less influence than natural light scarcity. Design responses should prioritise light management in spring and summer.

The study affirms that integrating vegetation with solar PV is feasible using light-zoned land-use planning, shade-tolerant species, and adaptive seasonal strategies. These practices can support Aotearoa New Zealand's goals for renewable energy and sustainable land use.

6.1. Recommendations for policy and practice

Several actionable recommendations arise from this work:

- Incorporate agronomic criteria into solar farm planning: Regulatory and permitting bodies should consider mandating vegetation-light modelling as part of environmental impact assessments for new PV farms, especially in agricultural zones.
- Encourage dual-use land strategies: This research supports national policies promoting land-use optimization. Integrating solar PV with grazing or shade-tolerant cropping could increase land efficiency and socio-ecological resilience.
- Establish vegetation monitoring baselines: Ongoing empirical studies at operational solar farms should monitor vegetation health, light variability, and species adaptation to inform future development guidelines.
- Site-specific light management: Developers should use light zoning maps to guide panel spacing, tilt, and layout adjustments that enable vegetative growth beneath or adjacent to arrays without compromising energy output.

6.2. Recommendations for further research

To build on this research, the following is recommended:

- A systematic sensitivity analysis should be conducted to explore how changes in panel tilt, azimuth, row spacing, and height affect light distribution. This would help identify key design parameters for maximizing both energy yield and vegetation productivity.

- Empirical validation using spectroradiometers or quantum sensors beneath installed PV panels is essential. Ground measurements at different seasons and times of day will help calibrate the model and adjust for real-world deviations, particularly during variable cloud conditions.
- Crop modelling tools could be integrated with light simulations to assess actual biomass or yield projections under modified light regimes. Model microclimate interactions (for example, evapotranspiration).
- Extending this analysis to different regions of Aotearoa New Zealand with varying climatic and ecological conditions.
- Undertake similar analyses for different technology configurations, especially single-axis tracking systems.

References

Adeh EH, Selker JS, Higgins CW, 2018. Remarkable agrivoltaic influence on soil moisture, micrometeorology, and water-use efficiency. Scientific Reports, 8(1), 1–10, doi:10.1038/s41598-018-28740-0.

Arksey HA, O'Malley, L, 2005. Scoping studies: towards a methodological framework. International Journal of Social Research Methodology, 19–32, doi:10.1080/1364557032000119616.

Bosch JL, López G, Batlles FJ, 2009. Global and direct photosynthetically active radiation parameterizations for clear-sky conditions. Agricultural and Forest Meteorology, 149(1), 146-158, doi:10.1016/j.agrformet.2008.07.011.

Brent AC, 2024. Agrivoltaic Systems for Aotearoa New Zealand. International Journal of Environmental Science and Natural Resources. doi:10.19080/IJESNR.2024.33.556357.

Brito C, Ferreira H, Dinis L-T, Trindade H, Marques D, Correia CM, Moutinho-Pereira J, 2023. Different LED light intensity and quality change perennial ryegrass (Lolium perenne L.) physiological and growth responses and water and energy consumption. Frontiers in Plant Science, 14, doi:10.3389/fpls.2023.1160100.

Brent AC, Iorns C, 2024. Solar farms can eat up farmland – but 'agrivoltaics' could mean the best of both worlds for NZ farmers. The Conversation, accessed 4 August 2025 from: https://theconversation.com/solar-farms-can-eat-up-farmland-but-agrivoltaics-could-mean-the-best-of-both-worlds-for-nz-farmers-230531.

Chen X, Chen B, Wang Y, Zhou N, Zhou Z, 2024. Response of vegetation and soil property changes by photovoltaic established stations based on a comprehensive meta-analysis. Land, 13(4), 478, doi:10.3390/land13040478.

Concept Consulting, 2023. Generation investment survey: 2023 update. Prepared for the Electricity Authority, accessed 4 August 2025 from: https://www.ea.govt.nz/documents/4414/Generation_Investment_Survey_-_2023_update.pdf.

Danny HW, Li JC, 2004. Predicting solar irradiance on inclined surfaces using sky radiance data. Energy Conversion and Management, 45, 1771–1781, doi:10.1016/j.enconman.2003.09.020.

Environmental Protection Authority, 2022. The application documents for the Tauhei Solar Farm. Wellington, accessed 3 August 2025 from: https://www.epa.govt.nz/fast-track-consenting/referred-projects/tauhei-solar-farm/the-application/.

Essery R, Marks D, 2007. Scaling and parametrization of clear-sky solar radiation over complex topography. Journal of Geophysical Research: Atmospheres, 112(D10), doi:10.1029/2006JD007650.

Fagnano M, Fiorentino N, Visconti D, Baldi GM, Falce M, Acutis M, Genovese M, Blasi MD, 2024. Effects of a photovoltaic plant on microclimate and crops' growth in a Mediterranean area. Agronomy, 14(3), 466, doi:10.3390/agronomy14030466.

Feistel U, Werisch S, Marx P, Kettner S, Ebermann J, Wagner L, 2022. Assessing the impact of shading by solar panels on evapotranspiration and plant growth using lysimeters. AIP Conference Proceedings, 2635, 150001, doi:10.1063/5.0103124.

Gu L, Baldocchi D, Verma SB, Black TA, Vesala T, Falge EM, Dowty PR, 2002. Advantages of diffuse radiation for terrestrial ecosystem productivity. Journal of Geophysical Research: Atmospheres, 107(D6), doi:10.1029/2001JD001242.

Gupta R, Kumar M, Tiwari R, Khare R, 2024. Effects of shading in agrivoltaic systems on maize yield: A case study. Applied Energy, 262(4), 114564. doi:10.1016/j.apenergy.2024.114564.

Hernandez RR, Easter SB, Murphy-Mariscal ML, Maestre FT, Tavassoli M, Allen EB, Allen MF, 2014. Environmental impacts of utility-scale solar energy. Renewable and Sustainable Energy Reviews, 29, 766–779, doi:10.1016/j.rser.2013.08.041.

Hickey T, 2023. Plant growth under photovoltaic arrays of varying transparencies – A study of plant response to light and shad-ow in agrivoltaic systems. Master's thesis, Colorado State University, Fort Collins, accessed 4 August 2025 from: https://hdl.handle.net/10217/236849.

Jedmowski C, Kherde S, Pahwa A, Schlechtrimen V, Meier-Grűll M, Muller O, 2022. Effect of shading in an agri-PV system on structure and growth of ornamental plants. AgriVoltaics Conference Proceedings,1, doi:10.52825/agripv.v1i.532.

Ko D-Y, Chae S-H, Moon H-W, Kim HJ, Seong J, Lee M-S, Ku K-M, 2023. Agrivoltaic farming insights: A case study on the cultivation and quality of kimchi cabbage and garlic. Agronomy, 13(10), 2625, doi:10.3390/agronomy13102625.

Laub M, Ehmann A, Weselek A, 2022. Impact of shading on crop yields: A meta-analysis of agrivoltaic systems. Renewable Energy, 150, 280–292, doi:10.1016/j.renene.2022.05.003.

Levac D, Colquhoun H, O'Brien KK, 2010. Scoping studies: Advancing the methodology. Implementation Science, 5(1), 69, doi:10.1186/1748-5908-5-69.

McArthur LJB, Hay JE, 1981. A technique for mapping the distribution of diffuse solar radiation over the sky hemisphere. Journal of Applied Meteorology and Climatology, 20(4), 421-429, doi:10.1175/1520-0450(1981)020%3C0421:ATFMTD%3E2.0.CO;2.

Marrou H, Guilioni L, Dufour L, Dupraz C, Wery J, 2013. Microclimate under agrivoltaic systems: Is crop growth hindered by the reduction in solar energy? Agricultural and Forest Meteorology, 177, 117–132, doi:10.1016/j.agrformet.2013.04.012.

Ministry of Business, Innovation & Employment (MBIE), 2023. Consultation document: Advancing New Zealand's energy transition. Wellington, accessed 4 August 2025 from: https://www.mbie.govt.nz/building-and-energy/energy-and-natural-resources/energy-consultations-and-reviews/advancing-new-zealands-energy-transition-consultation-document.

Ministry for the Environment (MfE), 2024. New Zealand's projected greenhouse gas emissions to 2050. Wellington, accessed 4 August 2025 from: https://environment.govt.nz/what-government-is-doing/areas-of-work/climate-change/emissions-reductions/emissions-reduction-targets/new-zealands-projected-greenhouse-gas-emissions-to-2050/.

Najafabadi, MK, 2024. Shade and light modelling for agrivoltaic systems – With focus on single-axis agrivoltaic systems. Lund University, accessed 4 August 2025 from: https://portal.research.lu.se/en/activities/shade-and-light-modeling-for-agrivoltaic-systems-with-focus-on-si.

Noor NFM, Reeza AA, 2022. Effects of solar photovoltaic installation on microclimate and soil properties in UiTM 50MWac solar park, Malaysia. IOP Conference Series: Earth and Environmental Science, 1059, doi:10.1088/1755-1315/1059/1/012031.

Oke TR, 1982. The energetic basis of the urban heat island. Quarterly Journal of the Royal Meteorological Society, 108(455), 1–24, accessed 4 August 2025 from: https://patarnott.com/pdf/Oake1982_UHI.pdf.

OpenAI, 2024. ChatGPT. Large language model, Version GPT-4o, accessed 23 September 2024 from: https://chat.openai.com.

Perez RS, 1987. A new simplified version of the Perez diffuse irradiance model for tilted surfaces. Solar Energy, 39(3), 221–231, doi:10.1016/S0038-092X(87)80031-2.

Perna A, 2021. Modeling and optimizing irradiance distributions in agrivoltaic systems. Master's thesis, Purdue University, accessed 4 August 2025 from: https://hammer.purdue.edu/ndownloader/files/17970563.

Photone, 2025. Light requirements for plants: Find your Plant's PPFD and DLI. Plant light database, accessed 11 August 2025 from: https://growlightmeter.com/light-requirements-for-plants/.

Potenza E, Croci M, Colauzzi M, Amaducci S, 2022. Agrivoltaic system and modelling simulation: A case study of soybean (Glycine max L.) in Italy. Horticulturae, 8(12), 1160, doi:10.3390/horticulturae8121160.

Quaschning V, Hanitsch R, 1995. Shade calculations in photovoltaic systems. ISES Solar World Conference. Harare, Zimbabwe, accessed 11 August 2025 from: https://www.researchgate.net/profile/Volker-Quaschning/publication/268519841_ISES1995/links/546f37d70cf216f8cfa9cb5b/ISES1995.pdf.

RED Horticulture, 2023. Measuring light in horticulture: PAR, PPF, and PPFD. Database, accessed 4 August 2025 from: https://www.horticulture.red/en/measuring-light-in-horticulture-par-ppf-and-ppfd/.

Sarr A, Soro YM, Tossa AK, Diop L, 2024. A new approach for modelling photovoltaic panel configuration maximizing crop yield and photovoltaic array outputs in agrivoltaics systems. Energy Conversion and Management, 309, 118436, doi:10.1016/j.enconman.2024.118436.

Scarano A, Semeraro T, Calisi A, Aretano R, Rotolo C, Lenucci MS, Santino A, De Caroli M, 2024. Effects of the agrivoltaic system on crop production: The case of tomato (Solanum lycopersicum L.). Applied Sciences, 14(7), 3095, doi:10.3390/app14073095.

SLR Consulting, 2024. Tauhei solar farm: Harmony Energy New Zealand. SLR Projects, accessed 11 August 2025 from: https://www.slrconsulting.com/projects/tauhei-solar-farm

Unruh JB, 2015. Daily light requirements for grass species. Lecture, University of Florida, accessed 11 August 2025 from: https://wfrec.ifas.ufl.edu/media/wfrecifasufledu/docs/pdf/turfgrass/Daily_Light_Requirements_Lawn_Grasses_FTGA_2015_Unruh.pdf.

van de Ven D-J, Capellan-Peréz I, Arto I, Cazcarro I, de Castro C, Patel P, Gonzalez-Eguino M, 2021. The potential land requirements and related land use change emissions of solar energy. Scientific Reports, 11, 2907, doi:10.1038/s41598-021-82042-5.

Vignola F, Peterson J, Kessler R, Snider S, Gotseff P, Sengupta M, Habte A, Andreas A, Mavromatakis F, 2021. Influence of diffuse and ground-reflected irradiance on the spectral modelling of solar reference cells. ASES National Solar Conference Proceedings, Boulder, Colorado, doi: 10.18086/solar.2021.01.06.

Weselek A, Ehmann A, Zikeli S, Lewandowski I, Schindele S, Högy P, 2019. Agrophotovoltaic systems: applications, challenges, and opportunities. A review. Agronomy for Sustainable Development, 39, 35, doi:10.1007/s13593-019-0581-3.

Xia X, 2014. A critical assessment of direct radiative effects of different aerosol types on surface global radiation and its components. Journal of Quantitative Spectroscopy and Radiative Transfer, 149, 72-80, doi:10.1016/j.jqsrt.2014.07.020.